# Tetracycline Adsorption from Aqueous Media by Magnetically Separable $Fe_3O_4$@Methylcellulose/APTMS (Isotherm, Kinetic and Thermodynamic Studies)

**Sobhan Maleky** ( sobhanmaleky@ymail.com )
Kerman University of Medical Sciences https://orcid.org/0000-0003-4143-3374
**Ali Asadipour**
Kerman University of Medical Sciences
**Alireza Nasiri**
Kerman University of Medical Sciences
**Rafael Luque**
University of Cordoba: Universidad de Cordoba
**Maryam Faraji**
Kerman University of Medical Sciences

**Research Article**

**Keywords:** Adsorption, 3-Aminopropyltrimethoxysilane, Methylcellulose, Tetracycline, Magnetic nano-biocomposite

**Posted Date:** December 15th, 2021

**DOI:** https://doi.org/10.21203/rs.3.rs-1115245/v1



**Version of Record:** A version of this preprint was published at Journal of Polymers and the Environment on April 2nd, 2022. See the published version at https://doi.org/10.1007/s10924-022-02428-y.

## Abstract

This study aimed to synthesize $Fe_3O_4$@Methylcellulose/3-Aminopropyltrimethoxysilane ($Fe_3O_4$@MC/APTMS) as a new magnetic nano-biocomposite by a facile, fast, and new microwave-assisted method and to be utilized as an adsorbent for tetracycline (TC) removal from aqueous solutions. $Fe_3O_4$@MC/APTMS was characterized by Fourier transform-infrared (FTIR), Field emission scanning electron microscopy (FESEM), Energy dispersive spectroscopy (EDS), Mapping, X-ray diffraction (XRD), Thermal gravimetric analysis (TGA), Brunauer–Emmett–Teller (BET) and vibrating sample magnetometer (VSM). The point of zero charge ($pH_{zpc}$) value of the nano-biocomposite was estimated to be 6.8 by the solid addition method. Optimum conditions were obtained in TC concentration: 10 mg $L^{-1}$, adsorbent dosage: 80 mg $L^{-1}$, contact time: 90 min, and solution pH: 6 with the maximum TC removal of 90% and 65.41% in synthetic and actual samples, respectively. The kinetic and isotherm equations pointed to a *pseudo*-second order kinetic and Langmuir isotherm optimum fitting models. Based on the values of entropy changes (ΔS) (50.04 J/mol k), the enthalpy changes (ΔH) (9.26 kJ/mol), and the negative Gibbs free energy changes (ΔG), the adsorption process was endothermic, random, and spontaneous. The synthesized adsorbent exhibited outstanding properties, including proper removal efficiency of TC, excellent reusability, and simple separation from aqueous media by a magnet. Consequently, it is highly desirable that $Fe_3O_4$@MC/APTMS magnetic nano-biocomposite could be used as a promising adsorbent for TC adsorption from aqueous solutions.


## Highlights

- $Fe_3O_4$@MC/APTMSas a new magnetic nano-biocomposite has been synthesized by a new microwave-assisted method and characterized with FESEM, EDS, Mapping, FT-IR, XRD, TGA, BET, and VSM techniques.
- The maximum removal efficiencies under optimal conditions (pH=6, TC concentration 10 mg $L^{-1}$, adsorbent dosage: 80 mg $L^{-1}$ and contact time: 90 min) for synthetic and actual samples were obtained 90% and 65.41%, respectively.
- Isotherm, kinetic and thermodynamic study of tetracycline adsorption were investigated.
- $Fe_3O_4$@MC/APTMS exhibited excellentreusability property up to 5 cycles.

## 1. Introduction

Over the last 30 years, pharmaceuticals have been regarded as one of the most important water pollutants because of their wide variety, consumption, and particular environmental resistance. These compounds are known as micropollutants, which can enter the environment from point sources such as sewage treatment plants and nonpoint sources such as herbicides, insecticides and excess fertilizers from agricultural lands [1–3]. Antibiotics have been categorized as emerging pollutants due to their negligent usage, continuous input, and persistence in various environmental matrices even at low concentrations [4]. Antibiotics consumption went up by 65% from 2000 to 2015. In 2017, United Nations (UN) experts warned that the improper disposal of antibiotics could produce the generation of "ferocious superbugs" [5]. Tetracyclines (TCs) are among the most consuming antibiotics and are produced by actinomycetes. These antibiotics can be divided into four groups, including oxytetracycline, tetracycline, chlortetracycline, doxycycline. They have been frequently used in human and veterinary medicines along with feed additives for several decades [6]. As a typical antibiotic, TC production and usage can be classified as the second rank worldwide. Approximately 70–90% of the primary TC is released into the environment over urine and feces due to their low biodegradability and stable chemical structure [7]. It was reported that TC concentration in the wastewater released from aquaculture farms up to 20 mg $L^{-1}$ [8]. Multiple methods have been reported to remove antibiotics including biological treatment [9], chlorination [10], advanced oxidation processes (AOPs) [11–13], electrochemical treatment [14], adsorption [3, 15–20], membrane processes [21], and ultrasonic cavitation effect method [22, 23]. AOPs may cause the formation of recalcitrant and ecotoxic oxidation by-products, which hinder their usage in wastewater treatment plants [24]. The use of membrane separation technologies has been limited due to fouling issues [25]. Conventional wastewater treatment plants (WWTPs) are not designed with the particular focus of removing pharmaceuticals. Stackelberg et al. [26] and Kulkarni et al. [27] reported that conventional WWTPs, mainly based on microorganisms, do not effectively destroy antibiotics due to their low concentrations in water and intricate molecular structure. The adsorption method has been regarded as the most successful technology to remove antibiotics from aqueous solutions owing to its low cost, high ef□ciency, and no risk of toxic by-products [6]. Several adsorbents, including activated carbons (ACs) [28], multi-walled carbon nanotubes (MWCNTs) [29], natural clay materials such as bentonite [30], ion exchange materials, and biochars (BCs), have been studied for antibiotic removal [31]. Methods based on nanotechnology are one of the newest methods to remove antibiotics. The application of nanomaterials is considered as fundamental for more efficient wastewater treatment [17, 32]. Nanoadsorbents have been reported as a new generation of adsorbents with higher adsorption capacity, making them more efficient for the adsorption of antibiotics and other emerging pollutants [15, 16, 18, 19, 31]. Furthermore, there are numerous nanoadsorbents used to remove antibiotics, including graphene-based nanoadsorbents [33], gold nanoparticles [34], zero-valent iron (ZVI) nanoparticles [35] and titanium dioxide nanoparticles [36]. Filtration and centrifugation methods are used to separate the non-magnetic adsorbents from an aqueous solution [37]. These techniques are time-consuming and require extra cost [38]. Magnetic adsorbents are a new class of adsorbents that could be used to remove drugs, heavy metals, oil, toxic organic compounds, dyes, and several biomolecules [39]. The production of magnetic adsorbents can solve this problem by assimilating magnetic nanoparticles on the adsorbent surfaces and their separation by the efficient, fast, and economical magnetic separation method [40, 41]. As the most abundant renewable biopolymer, Cellulose consists of three hydroxyl groups (-OH) per hydroglucose unit and is naturally produced about $10^{11}$–$10^{12}$ tons per year [42]. Cellulose-based nanomaterials are favorable adsorbents because of their high surface area-to-volume ratio, Affordability and intrinsic environmental inertness [43]. Cellulose-based adsorbents are fascinating materials, which could be readily adsorbed on the surfaces iron oxides such as $Fe_2O_3$ and $Fe_3O_4$ [44]. Cellulose

etherification is considered as the most important route for cellulose derivatization, and methylcellulose is one of the main cellulose ethers as well as carboxymethylcellulose (CMC). Besides, MC derivatives such as hydroxypropyl methylcellulose (HPMC), hydroxyethylcellulose (HEC), hydroxylpropyl cellulose (HPC), and ethylcellulose (EC) are conventionally used for coatings, films, membranes, drilling, pharmaceuticals, and foods [45, 46]. MC has numerous outstanding properties, including good solubility, high chemical stability, and is toxicologically innocuous [46]. Crude cellulose has low solubility, weak interaction with contaminants, low surface area, weak interaction with contaminants, and reuse problems [44]. The conjugation of MC with magnetic nanoparticles leads to more efficient biomagnetic adsorbents for removing organic contaminants in water and wastewater. [19]. Some properties of the cellulose-based adsorbents could be changed via modification [47]. Also, the surface of cellulose nanomaterials (CNs) is readily functionalizable, which allows for the cohesion of chemical portions that can enhance the binding efficiency of pollutants to the cellulose nanomaterials finally [43]. Cellulose-based nanomaterials are used to remove various toxic pollutants such as heavy metals, dyes, oil, pharmaceuticals, pesticides, and radioactive metals from aqueous solutions [44]. Besides, the application of different cellulose-based magnetic adsorbents such as $ZnFe_2O_4$@MC [19], $CoFe_2O_4$@MC, $ZnFe_2O_4$@CMC [2] and $CuFe_2O_4$@MC [3] for antibiotic adsorption has been studied recently. In general, chemical modification of cellulose materials results in higher adsorption capacities than unmodified cellulose forms [48]. 3-Aminopropyltrimethoxysilane (APTMS) is an organofunctional silane compound that contains amino groups. Silanization with coupling agents such as APTMS and 3-Aminopropyltriethoxysilane (APTES) has attracted extensive interest for the functionalization of nanoparticles with free amine groups [49]. Some studies reported that the surface modification of the nanoparticles could improve the mechanical properties of the coating. Palimi et al. [50] and Kegl et al. [51] Reported that surface modification by APTMS causes an enhancement in both hydrophobicity and removal efficiency.

This study has been aimed to synthesize a magnetic and eco-friendly nano-biocomposite for the removal of TC from aqueous solutions. Process parameters, including solution pH, initial concentration, adsorbent dosage, and contact time, were optimized, and adsorption isotherms, kinetics, and thermodynamics were investigated. The nano-biocomposite reusability and stability were also determined. To the best of our knowledge, $Fe_3O_4$@MC/APTMS has neither been synthesized nor used for the adsorption and removal of TC from aqueous solutions.

## 2. Materials And Methods

## 2.1. Chemicals and materials

TC ($C_{22}H_{24}N_2O_8$, 99%, 444.44 g $mol^{-1}$) was provided from Daroupakhsh Company (Tehran, Iran), Ferric chloride hexahydrate ($FeCl_3{\cdot}6H_2O$), Ferrous chloride ($FeCl_2$), methylcellulose, and sodium hydroxide (NaOH) were obtained from Merck (Germany), APTMS ($C_6H_{17}NO_3Si$, 95%) was obtained from ACROS (USA). Stock standard solution of TC at a concentration of 20 mg $L^{-1}$ was prepared with distilled water.

## 2.2. Preparation of $Fe_3O_4$@MC/APTMS

$Fe_3O_4$@MC/APTMS magnetic nano-biocomposite was prepared in two stages. In the first stage, stoichiometric amounts of metal chlorides and MC (10.8 g $FeCl_3$, 4 g $FeCl_2$, and 1 g MC) were dissolved in 100 mL of distilled water. NaOH (12 g) was added within 1h to alkalize the pH of the solution. Then, the suspension was placed in the microwave (SAMSUNG, 2450MHz, 800W) at 450 W for (3×5) min to obtain a dark brown precipitate. The obtained precipitate was separated using a magnet, washed several times with distilled water, and placed in an oven for 24h at 70°C. In the second stage of the synthesis, APTMS (4 mL) was dissolved in ethanol (50 mL). Next, the solution was added to the reaction container and stirred under reflux condition for 8h at 80°C to obtain $Fe_3O_4$@MC/APTMS as a product. The obtained residue was separated using a magnet and washed with distilled water to neutralize the final pH. Finally, the dark brown precipitate was dried for 24h at 25°C. The schematic of preparation of $Fe_3O_4$@MC/APTMS nano-biocomposite is shown in Fig. 1.

## 2.3. Characterization of synthesized $Fe_3O_4$@MC/APTMS

The surface morphology and elemental analysis of $Fe_3O_4$@MC/APTMS were examined by Field emission scanning electron microscope (FESEM, MIRA3TESCAN, Czech Republic) and the energy-dispersive X-ray spectroscopy (EDS) (MIRA2TESCAN, Czech Republic), respectively. Mapping of $Fe_3O_4$@MC/APTMS was obtained using a SAMX detector (MIRA II TESCAN, Czech Republic). The crystal structure of $Fe_3O_4$@MC/APTMS was investigated by X-ray diffraction (XRD) (PHILIPS, PW1730, Netherlands). The speci□c surface area and pore size distribution of $Fe_3O_4$@MC/APTMS were characterized by Brunauer-Emmett-Teller (BET) (BELSORP-mini II, JAPAN). The thermostability of synthesized adsorbent was investigated by a thermal gravimetric analyzer (TGA) (TA, Q600, USA). The magnetic properties of $Fe_3O_4$@MC/APTMS were surveyed by a vibrating sample magnetometer (VSM) (LBKFB, IRAN). The surface functional groups of $Fe_3O_4$@MC/APTMS were analyzed by Fourier transform infrared spectroscopy (FTIR) (Thermo, AVATAR, USA).

## 2.4. Batch adsorption experiments

Batch experiments were conducted to study the TC adsorption on synthesized $Fe_3O_4$@MC/APTMS in the synthetic solutions at room temperature in triplicates. A stock solution of TC was prepared by dissolving pure TC (0.02 g) in distilled water (100 mL). Different concentrations of TC used in batch experiments were obtained by diluting the individual stock solution. Specific amounts of adsorbent were added to a beaker containing 100 mL of the TC mixture. Suspensions were agitated by a magnetic stirrer at 300 rpm. Then, filtered using a 0.22 µm syringe filter (Jet Biofil), and the residual concentration of TC was measured at the maximum wavelength of 358 nm by UV/Vis spectrophotometer (Shimadzu 1800). We investigated the

effective parameters on the adsorption process, including solution pH (3, 5, 6, 9, and 11) that adjusted with 0.1 M HCl or NaOH with a pH meter (HANNA 211), adsorbent dosage (60, 80, 100, 120, and 150 mg $L^{-1}$), initial antibiotic concentration (5, 10, 15, 20, and 30 mg $L^{-1}$), contact time (20, 40, 60, 90, and 120 min), and temperature of the solution (298, 303, 308, 313, and 318 K). The removal efficiency of TC was calculated using Equation **1** [52]. The adsorption capacity at equilibrium ($q_e$) and amount of soption at time t ($q_t$) were calculated using Equations. **2** and **3**, respectively [20].

$$E = \frac{C_0 - C_e}{C_0} \quad (1)$$

$$q_e = (C_0 - C_e) \times \frac{V}{M} \quad (2)$$

$$q_t = (C_0 - C_t) \times \frac{V}{M} \quad (3)$$

Where $C_0$, $C_e$, and $C_t$ are TC concentrations (mg $L^{-1}$) at the initial time, equilibrium, and time t (min), respectively. V is the volume of the solution (L). M is the mass of the adsorbent (g).

Optimum conditions obtained from batch experiments on the synthetic solutions were investigated on the sanitary wastewater sample. High-performance liquid chromatography (HPLC) device (Shimadzu LC-10AD VP, Japan) was utilized to identify and measure TC concentration in the samples. Details of the HPLC analysis were included mobile phase: acetonitrile: deionized water 30:70 (v/v), column model: C18, 250×4.6 mm, 5 µm, detector: UV at the wavelength of 280 nm, injection volume: 20 µL at a flow rate of 1 mL $min^{-1}$ [53].

The adsorbent used in the experiments was reused for the subsequent cycles. After each run, the nanoadsorbent was separated by a magnet, washed several times with ethanol and distilled water, dried at 40°C, and reused in five runs.

## 2.5. Kinetics, isotherms, and thermodynamics studies

Langmuir, Freundlich, Temkin, and Dubinin-Radushkevich (D-R) isotherm models were employed to study isotherms of TC adsorption by $Fe_3O_4$@MC/APTMS at initial antibiotic concentrations of 5, 10, 15, 20, and 30 mg $L^{-1}$ at 25 ºC. *pseudo*-first order, *pseudo*-second order, Intraparticle, and Elovich were used to study the kinetics of TC adsorption by $Fe_3O_4$@MC/ APTMS at several contact times (5,10,15,20,40,60 and 90 min). To study the thermodynamic parameters of TC removal by $Fe_3O_4$@MC/APTMS at five different temperatures (298, 303, 308, 318, and 328 K), Equations **4** and **5** were used. In equation **4**, "ΔG" is Gibbs free energy changes, "R" is the gas constant with a value of 8.314 J/mol.K, "T" is the temperature of the reaction in Kelvin, and "$K_d$" is the equilibrium constant. In Equation **5**, "ΔS" is the standard entropy changes (kJ/mol), "ΔH" is the standard enthalpy changes (kJ/mol), and "R" is the ideal gas constant (J/mol. K). Both energy and entropy factors determine what processes would occur spontaneously [54, 55].

$$\Delta G = -RTLnK_d \quad (4)$$

$$LnKd = \frac{\Delta S}{R} - \frac{\Delta H}{RT} \quad (5)$$

# 3. Results And Discussion

## 3.1. $Fe_3O_4$@MC/APTMS magnetic nano-biocomposite characterization

A new microwave-assisted co-precipitation method was employed to synthesize magnetic $Fe_3O_4$@MC/APTMS nano-biocomposite. Microwave energy is well known to provide rapid heating determined by dielectric polarization of the given medium [56]. Several analytical techniques were employed to characterize the prepared magnetic nano-biocomposite.

Figure 2 illustrates a comparison of the KBr pellet FTIR spectra of MC, APTMS and $Fe_3O_4$@MC/APTMS using an FTIR spectrophotometer between 500 and 4000 $cm^{-1}$. According to the FTIR spectra of MC, the broad peak observed at 3461 $cm^{-1}$ was due to O-H stretching. In comparison, the peaks at 2931 $cm^{-1}$ and 1644 $cm^{-1}$ were related to asymmetric C-H stretching and adsorbed water stretching, respectively. Furthermore, the peaks at 1458.17 $cm^{-1}$ 1376.04 $cm^{-1}$ confirmed the C–H bending of methylene and methyl groups, respectively. Also, the C–O stretching was observed at 1100–1150 $cm^{-1}$ [57].

Moreover, in the FTIR spectra of APTMS, the broad peak at 3429 $cm^{-1}$ could be due to O–H stretching, while the peak at 2931 $cm^{-1}$ may be related to the asymmetric C–H stretching. The bands at ~1603 and ~1472 $cm^{-1}$ correspond to the bending mode of the N–H group. The bands appearing at ~1030 and ~774 $cm^{-1}$ could be assigned to vibrational modes in which bridging oxygen atoms participate in Si-O-Si and Si-O bonds. [58, 59].

In the FTIR spectra of $Fe_3O_4$@MC/APTMS, the peak at 3433 $cm^{-1}$ corresponded to the combined O–H and N–H stretching. The peaks at 2925 $cm^{-1}$ and 1634 $cm^{-1}$ corresponded to the $-CH_2$ and $-NH_2$, respectively, which proves the existence of the functionalized $NH_2$ groups on the $Fe_3O_4$@MC surface. Furthermore, the peak observed at 1384 $cm^{-1}$ corresponded to N–O bending. In 586 and 635 $cm^{-1}$ bands, two strong peaks can be attributed

to the stretching vibration mode, which corresponds to the Fe-O absorption band in the $Fe_3O_4$ crystal lattice [60]. Our findings are in good agreement with previous findings reported by Amirmahani et al. [59] and Palimi et al. [50].

Figure 3 depicts the morphology of the magnetic nano-biocomposite. FESEM images of $Fe_3O_4$@MC/APTMS illustrated the establishment of spherical-shaped nanoparticles (average particle size: ~52 nm). The surface morphology of the spherical $Fe_3O_4$@ MC/APTMS particles is compact, smooth, uniform and without agglomeration.

The EDS spectrum of $Fe_3O_4$@MC/APTMS is presented in Fig. 4a. The EDS of $Fe_3O_4$@MC/APTMS can define the chemical combination and pureness of the prepared magnetic nano-biocomposite. $Fe_3O_4$@MC/APTMS was composed of (73.38% Fe, 18.79% O, 5.45% C, 1.99% N and 0.39% Si). In this matter, the iron signal arose from the existence of the $Fe_3O_4$, the carbon signal derived from the presence of MC, and the nitrogen and silicon signal were attributed to the presence of APTMS in the $Fe_3O_4$@MC/APTMS nano-biocomposite. The results of EDS con□rmed the presence of the expected chemical composition of $Fe_3O_4$@MC/APTMS [40, 59].

Figure 4b represents the elemental mapping spectra of $Fe_3O_4$@MC/APTMS. The red, purple, yellow, green, and blue colors indicated the C, Fe, N, O and Si enriched areas of the nano-biocomposite, respectively. It could be mentioned that the elements were well-distributed in the nano-biocomposite, and the presence of Fe, O, C, Si, and N atoms confirmed the existence of $Fe_3O_4$@MC/APTMS.

The XRD analysis was done to identify the crystallinity and phase purity of the as-prepared nano-biocomposite. The XRD patterns of MC and $Fe_3O_4$@MC/APTMS are shown in Fig. 5. XRD patterns of MC exhibited an intense peak centered at 2θ = 18.23°. Also, the XRD patterns and crystal phase structure of $Fe_3O_4$@MC/APTMS showed peaks at 2θ values of 18.53°, 30.44°, 35.81°, 43.49°, 54.08°, 57.44°, 63°, and 74.94°. These peaks are in agreement with literature data (JCPDS 98-001-7122) and are evidence of the successful magnetic synthetic stage. Intriguingly, the XRD spectrum of $Fe_3O_4$@MC/APTMS determines characteristic peaks associated with both MC and $Fe_3O_4$@MC/APTMS, suggesting the successful synthesis of $Fe_3O_4$@MC/APTMS nano-biocomposite and demonstrating the crystal structure in reaction with MC and APTMS. Fe3O4 is well preserved.

Our results are in agreement with those obtained by Amirmahani et al.[59]. Also, the average particle size of $Fe_3O_4$@MC/ATPMS was found to be around 0.3 nm from the Scherrer equation (Equation **6**) [55].

$$D = \frac{0.9\lambda}{\beta cos\theta} \quad (6)$$

Where, D (nm), β, λ (nm) and $\theta$ are the particle diameter, the line broadening at half the maximum intensity X-ray wavelength and Bragg angle.

Concerning the importance of adsorbent thermal stability, the TGA of $Fe_3O_4$@MC/APTMS (Fig. 6) was carried out in a range from room temperature to 800°C (20°C/min). Thermal decomposition of $Fe_3O_4$@MC/APTMS took place in two stages. The □rst stage of weight loss of $Fe_3O_4$@MC/APTMS (~ 2%) could be ascribed to the adsorbed water loss in the temperature range of 50–200°C. About 8.5% weight loss happened at 200–600°C. It could be due to decomposition and the breaking bonds of MC and APTMS. According to the results, a total weight loss of 10.67% was observed in the nano-biocomposite at ~600°C, whereas no more weight loss was found up to 800°C. These results indicate the superb thermal resistance of $Fe_3O_4$@MC/APTMS.

The textural properties of the as-prepared magnetic nano-biocomposite were characterized by BET analysis. The BET, Barrett Joyner Halenda (BJH) adsorption-desorption isotherms of the as-prepared $Fe_3O_4$@MC/APTMS are shown in Fig. 7(a-c). The speci□c surface area of the $Fe_3O_4$@MC/APTMS magnetic nano-biocomposite was 67 $m^2$/g. The mean pore diameter and total pore volume ($p/p_0$ = 0.990) were 15.2 nm and 0.26 $cm^3$/g, respectively. The International Union of Pure and Applied Chemistry (IUPAC) reported that pores are divided into microporous, mesoporous, and macroporous materials. A mesoporous material is a nanoporous material consisting of pores with diameters between 2 and 50 nm. Furthermore, microporous and macroporous pore sizes are smaller than 2 nm and larger than 50 nm, respectively [16, 60]. Based on evaluating the BET specific area of $Fe_3O_4$@MC/APTMS, The synthesized magnetic adsorbent could be classified as a mesoporous material [2, 16].

In comparison to other magnetic adsorbents such as $MnFe_2O_4$/RGO (42 $m^2$/g) [61], $Fe_3O_4$/zeolite (64 $m^2$/g) [62], L-Cyst-$Fe_3O_4$ (58$m^2$/g) [63], and $CoFe_2O_4$/MMT (51$m^2$/g) [64], $Fe_3O_4$@MC/APTMS had a higher specific surface area (67$m^2$/g) that is a crucial factor for higher adsorption capacity. The magnetic properties of magnetic $Fe_3O_4$@MC/APTMS nano-biocomposite were measured by a vibrating sample magnetometer at room temperature, with the □eld sweeping from −15,000 to +15,000 Oe. It can be seen in Fig. 8 that the amounts of coercive force ($H_c$), saturation magnetization ($M_s$), and remnant magnetization ($M_r$) were 3.26 Oe, 65.18 emu/g, and 1.24 emu/g, respectively. These amounts confirmed sufficient magnetization power of $Fe_3O_4$@MC/APTMS nano-biocomposite for simple separation by external magnetic fields. Moreover, the prepared $Fe_3O_4$@MC/APTMS nano-biocomposite could be dispersed again in the water after removing the applied magnetic field.

**Effective parameters in TC adsorption by magnetic $Fe_3O_4$@MC/APTMS nano-biocomposite**

## 3.1.1. Effect of TC initial concentration

Variations in the removal ef□ciency of TC and its $q_e$ by the magnetic $Fe_3O_4$@MC/ATPMS nano-biocomposite at different concentrations of TC and contact times, solution pH of 6 and adsorbent dosage of 80 mg $L^{-1}$ are indicated in Fig. 9a.

As shown in Fig. 9a, with a growth in the initial TC concentration from 5 to 30 mg $L^{-1}$, the $q_e$ value increased from 5.7 to 24.04 mg $g^{-1}$. The initial concentration of TC provides a Significant driving force of concentration gradient to dominate the resistance force of mass transfer of TC among the solid and solution phase [61]. Conversely, an enhancement in the TC concentration reduced the removal ef□ciency from 91.36 to 64.11% (see Fig. 9b), owing to the decrease of available sites on the surface of adsorbent for TC adsorption [65].

Accordingly, the optimum TC concentration of 10 mg $L^{-1}$ was regarded as the optimum TC concentration. Before saturation of the nano-biocomposite surface, with an extension of the contact time to 90 min, the removal efficiency also increased. At low TC concentrations, the ratio of the initial amount of TC molecules to the available active sites of the magnetic adsorbent is low, which contributes to the high removal efficiency. As a result, at higher concentrations of TC, access to the adsorption sites is considerably limited and leading to less antibiotic adsorption. Our results are in good agreement with other studies conducted by Malakootian et al. [15] and Babaei et al. [66].

### 3.1.2. Effect of magnetic nano-biocomposite dosage

The optimal adsorbent dose is a crucial parameter that affects the amount of adsorbed adsorbate. As shown in Fig. 10, the removal efficiency was 78.02% for an adsorbent dosage of 60 mg $L^{-1}$. TC removal increased to 90% with an enhancement in the adsorbent dose to 80 mg $L^{-1}$. Further increase in the adsorbent dosage at its maximum level (150 mg $L^{-1}$) lead to a maximum removal efficiency of 92.45%. However, with 80 mg $L^{-1}$ of adsorbent dosage, the removal ef□ciency was almost constant, not remarkably different from the maximum level, and the adsorbent dosage of 80 mg $L^{-1}$ was selected as the optimum amount for subsequent experiments.

The removal efficiency increases with increasing adsorbent dosage due to the increased number of accessible active sites of the magnetic adsorbent, as previously reported in literature works [67, 68].

### 3.1.3. Effect of solution pH

The Solution pH is considered to be a key factor in the adsorption processes used to remove contaminants. In this study, variable pH ranges (3-11) were evaluated to determine the optimum pH for TC removal by $Fe_3O_4$@MC/APTMS. As Fig. 11a depicts, an enhancement in removal ef□ciency was observed with an increase in pH from 3 (73.84%) to 6 (89.81%), in opposition, more increase in pH from 6 to 11 (46.9%) lowered the removal efficiency significantly, owing to the electrostatic repulsion among TC and the negatively charged surface of the adsorbent which prevents adsorption.

The effect of solution pH can be explained by the $pH_{zpc}$ of the adsorbent. The $pH_{zpc}$ of $Fe_3O_4$@MC/APTMS was determined by the solid addition method and was found to be 6.8. As shown in Fig. 11b, TC has three acid dissociation constants (pKa), namely 3.3, 7.68, and 9.68. Consequently, depending on the pH value, it can form different ionic species by protonation or deprotonation. TC molecules are present in cationic (pH < 3.3), zwitterionic (3.3 < pH < 7.68), or anionic forms (pH > 7.68). It could be explained that at pH: 6, TC had both negative and positive charges. As mentioned above, the $pH_{zpc}$ value for $Fe_3O_4$@MC/APTMS was about 6.8, representing that it is positively charged at pH < 6.8, and electrostatic attraction occurs. In contrast, at pH > 6.8, the surface of $Fe_3O_4$@MC/APTMS is negatively charged, and electrostatic repulsion occurs, which hinders TC adsorption. Our results are in good agreement with previous studies [20, 69].

## 3.2. Adsorption isotherm studies

Isotherm models express the interaction among adsorbate and adsorbent at constant temperature [70]. The results of the isotherm study are mentioned in **Table 1**. The Langmuir model presumes that the adsorption takes place at a number of specific and uniform sites in the adsorbent. The Freundlich model is acquired by presuming a homogeneous surface with a distribution of irregularities of the adsorbed heat on the surface. The Temkin isothermal model is based on the fact that the heat from the sorption process of all molecules in the layer would decrease linearly. The D-R isotherm model is used to take into account the effect of the porous structure of adsorbents. It gives an understanding of the adsorbent porosity and the adsorption energy [70, 71].

According to **Table 1**, the linear regression coefficients of the Langmuir model were higher than other studied models ($R^2$=0.9918). The results were consistent with previous studies [15, 40, 69, 72].

The maximum adsorption capacity ($q_{max}$) and $K_L$ obtained from the Langmuir model were equal to 23.77 mg $g^{-1}$ and 0.71 L $mg^{-1}$, respectively. The dimensionless parameter of $R_L$ (0.21) was within the range of 0–1, which suggested that $Fe_3O_4$@MC/APTMS was a potential adsorbent for the removal of TC. The above results indicated that the TC adsorption was a monolayer sorption on a uniform adsorption surface between molecules with no interactions between molecules. [72, 73].

## 3.3. Kinetic models

Kinetic models are employed to study the adsorption mechanisms. Adsorption is a Physico-chemical process in which the adsorbate is transferred from the solution phase to the surface of the adsorbent. Different kinetic models can be utilized to describe the transfer behavior of the adsorbate molecules [71].

Table 2 summarizes the properties of each model. As shown in Fig. 12a, the TC adsorption by $Fe_3O_4$@MC/APTMS is well fitted on the *pseudo*-second-order kinetic model ($R^2$ = 0.98).

Table 1
Parameters from the pseudo-first order, pseudo-second order, Intraparticle and Elovich kinetic models

| Model | Formula | Linear form | Plot | Parameter | Value |
|---|---|---|---|---|---|
| Langmuir | $q_e = q_m .b.C_e/1 + k_L. C_e$ | $C_e/q_e = C_e/q_m + 1/q_m. k_L$ | $C_e/q_e$ vs. $C_e$ | $q_{max}$ (mg $g^{-1}$) | 23.77 |
| | | | | $k_L$ (L/mg) | 0.71 |
| | | | | $R^2$ | 0.992 |
| Freundlich | $q_e = k_f C_e^{1/n}$ | Log $q_e$ = log $k_f$ + 1/n log $C_e$ | log $q_e$ vs. log $C_e$ | $K_f$ (L/mg) | 9.14 |
| | | | | n | 2.29 |
| | | | | $R^2$ | 0.96 |
| Temkin | $q_e$ = RT/b ln ($k_f.C_e$) | $q_e = B_1$ ln $k_f + B_1$ ln $C_e$ | $q_e$ vs.ln $C_e$ | $K_t$ (L/mg) | 6.09 |
| | | | | $B_1$ | 5.56 |
| | | | | $R^2$ | 0.990 |
| Dubinin-Radushkevich | $q_e = q_m$ exp. ($-B.\varepsilon^2$) | Ln $q_e$ = ln $q_m - B. \varepsilon^2$ | Ln $q_e$ vs. $\varepsilon^2$ | $q_{max}$ (mg $g^{-1}$) | 7.92 |
| | | | | E (kJ/mol) | 54.21 |
| | | | | $R^2$ | 0.9 |

These results implied that the adsorption process of TC by $Fe_3O_4$@MC/APTMS was the rate-controlling limiting step. The value of $q_e$ estimated by the *pseudo*-second-order kinetic model was 11.45 mg $g^{-1}$ and the calculated rate constant $k_2$ was found to be 0.011 g $mg^{-1}$ $min^{-1}$. The obtained kinetic model fitting is consistent with the previous studies conducted for the adsorptive removal of various pollutants by different adsorbents [40, 74].

Changes in the TC adsorption spectra due to the adsorption process are shown in Fig. 12b at various contact times. The TC adsorption peak is observed at 358 nm. The reduction in the intensity of adsorption peak by increasing the contact time indicated TC removal during the adsorption process.

## 3.4. Thermodynamic evaluation of the Tetracycline adsorption process

The thermodynamic parameters of TC adsorption by the studied magnetic nano-biocomposite have been summarized in Table 3. Positive ΔH and Δ*S* values indicated that the adsorption process of TC was endothermic and random, respectively. Negative ΔG values pointed to a spontaneous process [75]. ΔG values decreased at increased temperatures, indicating that the spontaneity increased at the higher temperatures [76]. These results are consistent with previously reported literature works [40, 72, 77].

Table 2

Parameters from the pseudo-first order, pseudo-second order, Intraparticle and Elovich kinetic models

| Model | Formula | Plot | Parameter | Value |
|---|---|---|---|---|
| *pseudo*-first order | $\log(q_e-q_t) = \log q_e - K_1.t$ | $\log (q_e-q_t)$ vs. t | $K_1$ ($min^{-1}$) | -0.0006 |
| | | | $q_e$ (mg $g^{-1}$) | 11.01 |
| | | | $R^2$ | 0.722 |
| *pseudo*-second order | $t/q_t = 1/K_2.q_e + (t/q_e)$ | $t/q_t$ vs. $t$ | $K_2$ ($min^{-1}$) | 0.01 |
| | | | $q_e$ (mg $g^{-1}$) | 11.45 |
| | | | $R^2$ | 0.98 |
| Intraparticle | $q_t = k_P .t^{0.5} + c$ | $q_t$ vs. $t^{0.5}$ | $K_P$ (mg/g $min^{-0.5}$) | 1.55 |
| | | | C (mg $g^{-1}$) | 3.56 |
| | | | $R^2$ | 0.96 |
| Elovich | $q_t = 1/\beta \ln(\alpha.\beta) + 1/\beta \ln t$ | $q_t$ vs. Ln $t$ | β (g $mg^{-1}$) | 0.64 |
| | | | α (mg/g $min^{-1}$) | 14.77 |
| | | | $R^2$ | 0.93 |

## 3.5. Recovery of $Fe_3O_4$@MC/APTMS

The reusability is a significant factor in terms of practical applications of as-prepared magnetic nano-biocomposite. The results of the recovery study are shown in Fig. 13. The results showed that the adsorptive activity of $Fe_3O_4$@MC/APTMS reduced was to 81.35% after the second run. The adsorption percentage decrease can be driven by the adsorption of intermediates on the magnetic nano-biocomposite active sites, making them unavailable to remove a fresh TC solution [19]. However, after five runs, 74% of the TC could be successfully adsorbed.

## 3.6. TC removal from actual wastewater

The optimal conditions determined through the synthetic samples were investigated on the sanitary wastewater collected from the Kerman University of Medical Sciences campus. The Wastewater sample was collected from the chlorination unit inlet. Under optimum conditions, the maximum TC removal ef□ciency was found to be 65%. The decrease in removal efficiency compared to synthetic conditions could be described by the presence of wastewater anions and cations. Interfering factors such as cyclic and organic compounds along with turbidity in the wastewater led to a decrease in the TC removal efficiency in the actual samples, as previously reported [2, 19]. The physicochemical characteristics of the employed actual wastewater sample included BOD (58 mg $L^{-1}$), COD (107.4 mg $L^{-1}$), TSS (16 mg $L^{-1}$), TDS (1040 mg $L^{-1}$), Nitrate (1 mg $L^{-1}$), $PO_4$ (35.31 mg $L^{-1}$), pH (7.57), and TC concentration (9.55 mg $L^{-1}$).

## 3.7. Adsorption mechanism

FTIR analysis of $Fe_3O_4$@ MC/APTMS before and after TC adsorption was compared in Fig. 14. It could be observed some differences in the FTIR spectra before and after TC adsorption due to TC binding on the surface of the adsorbent. After the adsorption process, the peaks at 2925 $cm^{-1}$ and 1634 $cm^{-1}$, which corresponded to –OH and $–NH_2$ groups, shifted to a lower wavelength and intensity (2922 $cm^{-1}$ for –OH group and 1630 $cm^{-1}$ for $–NH_2$ group). Moreover, the peaks at 1060 $cm^{-1}$, 635 $cm^{-1}$ and 459 $cm^{-1,}$ which were related to Si–O, Fe–O and Si–O–Si functional groups, shifted to 997 $cm^{-1}$, 632 $cm^{-1}$ and 443 $cm^{-1,}$ respectively. As a result, it could be stated that the –CH, $–NH_2$, Si–O, Fe–O and Si–O–Si groups had participated in the adsorption process of TC by the $Fe_3O_4$@MC/APTMS magnetic nano-biocomposite and the $Fe_3O_4$@ MC/APTMS bands relative intensity decreased.

A comparison of $Fe_3O_4$@MC/APTMS to other nanoadsorbents is presented in Table 4. $Fe_3O_4$@MC/APTMS synthesized and used in the current study showed an acceptable performance in terms of the maximum adsorption capacity ($q_{max}$), removal efficiency, Reusability, contact time and adsorbent usage.

**Table 3**

The thermodynamic parameters of TC adsorption by the studied magnetic nano-biocomposite

| Temp (K) | 1/T | $K_d$ | $lnK_d$ | $\Delta G°$ (KJ $mol^{-1}$) | $\Delta S°$ (J/mol K) | $\Delta H°$ (KJ $mol^{-1}$) |
|---|---|---|---|---|---|---|
| 298 | 0.00336 | 9.90 | 2.29 | -5.68 | | |
| 308 | 0.00325 | 10.98 | 2.39 | -6.13 | 50.04 | 9.24 |
| 318 | 0.00314 | 12.55 | 2.52 | -6.68 | | |
| 328 | 0.00305 | 13.84 | 2.62 | -7.16 | | |

**Table 4**

Comparison of the performance of $Fe_3O_4$@MC/APTMS with other nanoadsorbents

| Adsorbent | Dosage ($gL^{-1}$) | Antibiotic | Optimum pH | Optimum Time (min) | Removal efficiency in synthetic solution (%) | Removal efficiency in real sample (%) | Reusability | $q_{max}$(mg $g^{-1}$) | Reference |
|---|---|---|---|---|---|---|---|---|---|
| Mag-SBE@C | 2.21 | Tetracycline | 6.53 | 1440 | 99.9 | - | 4 cycles | 0.238 ($mmolg^{-1}$) | [78] |
| Au-$TiO_2$@$ZnFe_2O_4$ | 1 | Tetracycline | 5.1 | 240 | 87 | - | 3 cycles | - | [79] |
| $ZnFe_2O_4$/Ag/PEDOT | 0.002 | Tetracycline | 5.93 | 120 | 71.77 | - | - | 1.47 | [80] |
| Fe-modified sepiolite | 0.2 | Metronidazole | 7 | 15 | 36.6 | - | - | 5.62 | [81] |
| Nanocellulose | 1.5 | Tetracycline | 5 | 120 | 79.3 | - | 3 cycles | 7.73 | [82] |
| $Fe_3O_4$ -chitosan MIPs | 0.01 | Sulfamethoxazole | 4 | 30 | - | - | 6 cycles | 4.32 | [83] |
| CNCs-GO | 1 | Levofloxacin | 4 | 240 | 80 | - | - | 23.28 | [84] |
| $Fe_3O_4$@MC/APTMS | 0.08 | Tetracycline | 6 | 90 | 90 | 65 | 5 cycles | 23.77 | Current study |

# 4. Conclusion

$Fe_3O_4$@MC/APTMS was prepared by the microwave-assisted co-precipitation method in aqueous media. FESEM, EDS, Mapping, FT-IR, XRD, TGA, BET, and VSM techniques were carried out to identify the structure of as-prepared $Fe_3O_4$@MC/APTMS magnetic nano-biocomposite. $S_{BET}$ and the mean pore size of the adsorbent were 67 $m^2$/g and 15.2 nm, respectively. Furthermore, the synthesized adsorbent represented excellent thermal stability as well as good magnetic properties with a saturation magnetization of 65.18 emu/g. $q_{max}$ of the synthesized $Fe_3O_4$@MC/APTMS for TC adsorption was obtained 23.77 mg $g^{-1}$. The adsorption data of TC were well fitted on the Langmuir isotherm model. Kinetic studies exhibited that the adsorption process followed the *pseudo*-second-order kinetic model. $Fe_3O_4$@MC/APTMS as a new nano-biocomposite can be utilized as an environment-friendly bioadsorbent to remove TC with high efficiency from aqueous solutions, as well as convenient and straightforward magnetic separation. Our findings may offer a new strategy to prepare high-performance magnetic biopolymer-based and amino-functionalized bioadsorbents to remove various water and wastewater pollutants such as dyes, heavy metals and other pharmaceutical compounds.

# Declarations


### Acknowledgments

This research was part of a Master of Science thesis of Sobhan Maleky, a student of Environmental HealthEngineering in Kerman University of Medical Sciences. This work was supported by the Vice-Chancellor for Research and Technology of Kerman University of Medical Sciences under grant number 99001100 and the code of research ethics certificate IR.KMU.REC.1400.004. The authors would like to acknowledge the Environmental Health Engineering Research Center of Kerman University of Medical Sciences.


### Declaration of interest statement

The authors declare that they have no known competing financial interests or personal relationships that could have appeared to influence the work reported in this paper.


### Funding

This work was supported by the Vice-Chancellor for Research and Technology of Kerman University of Medical Sciences under grant number 99001100 and the code of research ethics certificate IR.KMU.REC.1400.004.


### Competing Interests

The authors declare that they have no known competing financial interests or personal relationships that could have appeared to influence the work reported in this paper.

### Author Contributions

*All authors contributed to the study conception and design. Material preparation, data collection and analysis were performed by [Sobhan Maleky], [Alireza Nasiri], [Maryam Faraji], [Ali Asadipour] and [Rafael Luque]. The first draft of the manuscript was written by [Sobhan Maleky] and all authors commented on previous versions of the manuscript. All authors read and approved the final manuscript.*All authors read and approved the final manuscript.

### Data Availability

*The datasets generated during and/or analyzed during the current study are available from the corresponding author on reasonable request.*

## References


[1] E. Asgari, A. Sheikhmohammadi, J. Yeganeh, (2020) Application of the Fe3O4-chitosan nano-adsorbent for the adsorption of metronidazole from wastewater: Optimization, kinetic, thermodynamic and equilibrium studies, International Journal of Biological Macromolecules, 164 694-706.https://doi.org/10.1016/j.ijbiomac.2020.07.188

[2] M. Malakootian, A. Nasiri, A. Asadipour, E. Kargar, (2019) Facile and green synthesis of ZnFe2O4@CMC as a new magnetic nanophotocatalyst for ciprofloxacin degradation from aqueous media, Process Safety and Environmental Protection, 129 138-151.https://doi.org/10.1016/j.psep.2019.06.022

[3] F. Tamaddon, A. Nasiri, G. Yazdanpanah, (2020) Photocatalytic degradation of ciprofloxacin using CuFe2O4@methyl cellulose based magnetic nanobiocomposite, MethodsX, 7 100764.https://doi.org/10.1016/j.mex.2019.12.005

[4] N. Das, J. Madhavan, A. Selvi, D. Das, (2019) An overview of cephalosporin antibiotics as emerging contaminants: a serious environmental concern, 3 Biotech, 9 231.10.1007/s13205-019-1766-9

[5] B.L. Phoon, C.C. Ong, M.S. Mohamed Saheed, P.-L. Show, J.-S. Chang, T.C. Ling, S.S. Lam, J.C. Juan, (2020) Conventional and emerging technologies for removal of antibiotics from wastewater, Journal of Hazardous Materials, 400 122961.https://doi.org/10.1016/j.jhazmat.2020.122961

[6] Y. Zhang, Z. Jiao, Y. Hu, S. Lv, H. Fan, Y. Zeng, J. Hu, M. Wang, (2017) Removal of tetracycline and oxytetracycline from water by magnetic Fe(3)O(4)@graphene, Environ Sci Pollut Res Int, 24 2987-2995.10.1007/s11356-016-7964-7

[7] M. Minale, Z. Gu, A. Guadie, D.M. Kabtamu, Y. Li, X. Wang, (2020) Application of graphene-based materials for removal of tetracyclines using adsorption and photocatalytic-degradation: A review, Journal of Environmental Management, 276 111310.https://doi.org/10.1016/j.jenvman.2020.111310

[8] W. Xiong, Z. Zeng, G. Zeng, Z. Yang, R. Xiao, X. Li, J. Cao, C. Zhou, H. Chen, M. Jia, Y. Yang, W. Wang, X. Tang, (2019) Metal-organic frameworks derived magnetic carbon-αFe/Fe3C composites as a highly effective adsorbent for tetracycline removal from aqueous solution, Chemical Engineering Journal, 374 91-99.https://doi.org/10.1016/j.cej.2019.05.164

[9] O.A. Arikan, (2008) Degradation and metabolization of chlortetracycline during the anaerobic digestion of manure from medicated calves, Journal of Hazardous Materials, 158 485-490.https://doi.org/10.1016/j.jhazmat.2008.01.096

[10] S. Navalon, M. Alvaro, H. Garcia, (2008) Reaction of chlorine dioxide with emergent water pollutants: Product study of the reaction of three β-lactam antibiotics with ClO2, Water Research, 42 1935-1942.https://doi.org/10.1016/j.watres.2007.11.023

[11] M. Malakootian, H. Mahdizadeh, M. Khavari, A. Nasiri, M.A. Gharaghani, M. Khatami, E. Sahle-Demessie, R.S. Varma, (2020) Efficiency of novel Fe/charcoal/ultrasonic micro-electrolysis strategy in the removal of Acid Red 18 from aqueous solutions, Journal of Environmental Chemical Engineering, 8.10.1016/j.jece.2019.103553

[12] M. Malakootian, A. Nasiri, A. Alibeigi, H. Mahdizadeh, M. Gharaghani, (2019) Synthesis and stabilization of ZnO nanoparticles on a glass plate to study the removal efficiency of acid red 18 by hybrid advanced oxidation process (ultraviolet/ZnO/ultrasonic), DESALINATION AND WATER TREATMENT, 170 325-336.10.5004/dwt.2019.24728

[13] M. Malakootian, A. Smith, Jr., M.A. Gharaghani, H. Mahdizadeh, A. Nasiri, G. Yazdanpanah, (2020) Decoloration of textile Acid Red 18 dye by hybrid UV/COP advanced oxidation process using ZnO as a catalyst immobilized on a stone surface, Desalination and Water Treatment, 182 385-394.10.5004/dwt.2020.25216

[14] J. Hirose, F. Kondo, T. Nakano, T. Kobayashi, N. Hiro, Y. Ando, H. Takenaka, K. Sano, (2005) Inactivation of antineoplastics in clinical wastewater by electrolysis, Chemosphere, 60 1018-1024.https://doi.org/10.1016/j.chemosphere.2005.01.024

[15] M. Malakootian, A. Nasiri, H. Mahdizadeh, (2018) Preparation of CoFe(2)O(4)/activated carbon@chitosan as a new magnetic nanobiocomposite for adsorption of ciprofloxacin in aqueous solutions, Water Sci Technol, 78 2158-2170.10.2166/wst.2018.494

[16] M. Malakootian, A. Nasiri, H. Mahdizadeh, (2019) Metronidazole adsorption on CoFe2O4/activated carbon@ chitosan as a new magnetic biocomposite: modelling, analysis, and optimization by response surface methodology,

[17] A. Nasiri, F. Tamaddon, M.H. Mosslemin, M. Faraji, (2019) A microwave assisted method to synthesize nanoCoFe2O4@methyl cellulose as a novel metal-organic framework for antibiotic degradation, MethodsX, 6.10.1016/j.mex.2019.06.017

[18] A. Nasiri, F. Tamaddon, M.H. Mosslemin, M.A. Gharaghani, A. Asadipour, (2019) New magnetic nanobiocomposite CoFe2O4@methycellulose: facile synthesis, characterization, and photocatalytic degradation of metronidazole, Journal of Materials Science: Materials in Electronics, 30 8595-8610.10.1007/s10854-019-01182-7

[19] F. Tamaddon, M.H. Mosslemin, A. Asadipour, M.A. Gharaghani, A. Nasiri, (2020) Microwave-assisted preparation of ZnFe(2)O(4)@methyl cellulose as a new nano-biomagnetic photocatalyst for photodegradation of metronidazole, Int J Biol Macromol, 154 1036-1049.10.1016/j.ijbiomac.2020.03.069

[20] A. Nasiri, M. Malakootian, M.A. Shiri, G. Yazdanpanah, M. Nozari, (2021) $CoFe_2O_4$@methylcellulose synthesized as a new magnetic nanocomposite to tetracycline adsorption: modeling, analysis, and optimization by response surface methodology, Journal of Polymer Research, 28.10.1007/s10965-021-02540-y

[21] I. Koyuncu, O.A. Arikan, M.R. Wiesner, C. Rice, (2008) Removal of hormones and antibiotics by nanofiltration membranes, Journal of Membrane Science, 309 94-101.https://doi.org/10.1016/j.memsci.2007.10.010

[22] W. Guo, Y. Shi, H. Wang, H. Yang, G. Zhang, (2010) Intensification of sonochemical degradation of antibiotics levofloxacin using carbon tetrachloride, Ultrasonics Sonochemistry, 17 680-684.https://doi.org/10.1016/j.ultsonch.2010.01.004

[23] N. Khoshnamvand, A. Jafari, B. Kamarehie, M. Faraji, (2019) Optimization of adsorption and sonocatalytic degradation of fluoride by zeolitic imidazole framework-8 (ZIF-8) using RSM-CCD, DESALINATION AND WATER TREATMENT, 171 270-280.10.5004/dwt.2019.24775

[24] K.G. Linden, M. Mohseni, 2.8 - Advanced Oxidation Processes: Applications in Drinking Water Treatment, in: S. Ahuja (Ed.) Comprehensive Water Quality and Purification, Elsevier, Waltham, 2014, pp. 148-172.

[25] T. Wang, X. Pan, W. Ben, J. Wang, P. Hou, Z. Qiang, (2017) Adsorptive removal of antibiotics from water using magnetic ion exchange resin, Journal of Environmental Sciences, 52 111-117.https://doi.org/10.1016/j.jes.2016.03.017

[26] P.E. Stackelberg, E.T. Furlong, M.T. Meyer, S.D. Zaugg, A.K. Henderson, D.B. Reissman, (2004) Persistence of pharmaceutical compounds and other organic wastewater contaminants in a conventional drinking-water-treatment plant, Sci Total Environ, 329 99-113.10.1016/j.scitotenv.2004.03.015

[27] P. Kulkarni, N.D. Olson, G.A. Raspanti, R.E. Rosenberg Goldstein, S.G. Gibbs, A. Sapkota, A.R. Sapkota, (2017) Antibiotic Concentrations Decrease during Wastewater Treatment but Persist at Low Levels in Reclaimed Water, Int J Environ Res Public Health, 14 668.10.3390/ijerph14060668

[28] G. Kaur, N. Singh, A. Rajor, (2021) Adsorption of doxycycline hydrochloride onto powdered activated carbon synthesized from pumpkin seed shell by microwave-assisted pyrolysis, Environmental Technology & Innovation, 23 101601.https://doi.org/10.1016/j.eti.2021.101601

[29] D.H. Carrales-Alvarado, R. Leyva-Ramos, I. Rodríguez-Ramos, E. Mendoza-Mendoza, A.E. Moral-Rodríguez, (2020) Adsorption capacity of different types of carbon nanotubes towards metronidazole and dimetridazole antibiotics from aqueous solutions: effect of morphology and surface chemistry, Environmental Science and Pollution Research, 27 17123-17137.10.1007/s11356-020-08110-x

[30] M.E. Mahmoud, A.M. El-Ghanam, R.H.A. Mohamed, S.R. Saad, (2020) Enhanced adsorption of Levofloxacin and Ceftriaxone antibiotics from water by assembled composite of nanotitanium oxide/chitosan/nano-bentonite, Materials Science and Engineering: C, 108 110199.https://doi.org/10.1016/j.msec.2019.110199

[31] M.B. Ahmed, J.L. Zhou, H.H. Ngo, W. Guo, (2015) Adsorptive removal of antibiotics from water and wastewater: Progress and challenges, Sci Total Environ, 532 112-126.10.1016/j.scitotenv.2015.05.130

[32] M. Malakootian, M. Yaseri, M. Faraji, (2019) Removal of antibiotics from aqueous solutions by nanoparticles: a systematic review and meta-analysis, Environmental Science and Pollution Research, 26 8444-8458.10.1007/s11356-019-04227-w

[33] T. Huang, X. Tang, K. Luo, Y. Wu, X. Hou, S. Tang, (2021) An overview of graphene-based nanoadsorbent materials for environmental contaminants detection, TrAC Trends in Analytical Chemistry, 139 116255.https://doi.org/10.1016/j.trac.2021.116255

[34] L. Qin, Z. Wang, Y. Fu, C. Lai, X. Liu, B. Li, S. Liu, H. Yi, L. Li, M. Zhang, Z. Li, W. Cao, Q. Niu, (2021) Gold nanoparticles-modified MnFe(2)O(4) with synergistic catalysis for photo-Fenton degradation of tetracycline under neutral pH, J Hazard Mater, 414 125448.10.1016/j.jhazmat.2021.125448

[35] H. Zhou, Z. Cao, M. Zhang, Z. Ying, L. Ma, (2021) Zero-valent iron enhanced in-situ advanced anaerobic digestion for the removal of antibiotics and antibiotic resistance genes in sewage sludge, Science of The Total Environment, 754 142077.https://doi.org/10.1016/j.scitotenv.2020.142077

[36] X. Sun, W. He, T. Yang, H. Ji, W. Liu, J. Lei, Y. Liu, Z. Cai, (2021) Ternary TiO2/WO3/CQDs nanocomposites for enhanced photocatalytic mineralization of aqueous cephalexin: Degradation mechanism and toxicity evaluation, Chemical Engineering Journal, 412 128679.https://doi.org/10.1016/j.cej.2021.128679

[37] O. Duman, S. Tunç, B.K. Bozoğlan, T.G. Polat, (2016) Removal of triphenylmethane and reactive azo dyes from aqueous solution by magnetic carbon nanotube-κ-carrageenan-Fe3O4 nanocomposite, Journal of Alloys and Compounds, 687 370-383.https://doi.org/10.1016/j.jallcom.2016.06.160

[38] O. Duman, C. Özcan, T. Gürkan Polat, S. Tunç, (2019) Carbon nanotube-based magnetic and non-magnetic adsorbents for the high-efficiency removal of diquat dibromide herbicide from water: OMWCNT, OMWCNT-Fe3O4 and OMWCNT-κ-carrageenan-Fe3O4 nanocomposites, Environmental Pollution, 244 723-732.https://doi.org/10.1016/j.envpol.2018.10.071

[39] O.V. Kharissova, H.V.R. Dias, B.I. Kharisov, (2015) Magnetic adsorbents based on micro- and nano-structured materials, RSC Advances, 5 6695-6719.10.1039/C4RA11423J

[40] M. Hosseinzehi, M.H. Ehrampoush, F. Tamaddon, M. Mokhtari, A. Dalvand, (2021) Eco-environmental preparation of magnetic activated carbon modified with 3-aminopropyltrimethoxysilane (APTMS) from sawdust waste as a novel efficient adsorbent for humic acid removal: Characterisation, modelling, optimisation and equilibrium studies, International Journal of Environmental Analytical Chemistry, 1-21.10.1080/03067319.2021.1928096

[41] H. Sereshti, O. Duman, S. Tunç, N. Nouri, P. Khorram, (2020) Nanosorbent-based solid phase microextraction techniques for the monitoring of emerging organic contaminants in water and wastewater samples, Microchimica Acta, 187 541.10.1007/s00604-020-04527-w

[42] R. Jiang, H.-Y. Zhu, Y.-Q. Fu, E.-M. Zong, S.-T. Jiang, J.-B. Li, J.-Q. Zhu, Y.-Y. Zhu, (2021) Magnetic NiFe2O4/MWCNTs functionalized cellulose bioadsorbent with enhanced adsorption property and rapid separation, Carbohydrate Polymers, 252 117158.https://doi.org/10.1016/j.carbpol.2020.117158

[43] A.W. Carpenter, C.F. de Lannoy, M.R. Wiesner, (2015) Cellulose nanomaterials in water treatment technologies, Environ Sci Technol, 49 5277-5287.10.1021/es506351r

[44] D. Mohamed, A. Dhamodaran, Magnetic Cellulose Green Nanocomposite Adsorbents for the Removal of Heavy Metal Ions in Water/Wastewater, in, 2019.

[45] R. Ergun, J. Guo, B. Huebner-Keese, Cellulose, in: B. Caballero, P.M. Finglas, F. Toldrá (Eds.) Encyclopedia of Food and Health, Academic Press, Oxford, 2016, pp. 694-702.

[46] D. Klemm, B. Heublein, H.-P. Fink, A. Bohn, (2005) Cellulose: Fascinating Biopolymer and Sustainable Raw Material, Angewandte Chemie International Edition, 44 3358-3393.https://doi.org/10.1002/anie.200460587

[47] D. Trache, A.F. Tarchoun, M. Derradji, T.S. Hamidon, N. Masruchin, N. Brosse, M.H. Hussin, (2020) Nanocellulose: From Fundamentals to Advanced Applications, Front Chem, 8 392-392.10.3389/fchem.2020.00392

[48] S. Hokkanen, A. Bhatnagar, M. Sillanpää, (2016) A review on modification methods to cellulose-based adsorbents to improve adsorption capacity, Water Research, 91 156-173.https://doi.org/10.1016/j.watres.2016.01.008

[49] A. Jain, G.A. Hirata, M.H. Farías, F.F. Castillón, (2016) Synthesis and characterization of (3-Aminopropyl)trimethoxy-silane (APTMS) functionalized Gd2O3:Eu(3+) red phosphor with enhanced quantum yield, Nanotechnology, 27 065601.10.1088/0957-4484/27/6/065601

[50] M.J. Palimi, M. Rostami, M. Mahdavian, B. Ramezanzadeh, (2014) Surface modification of Fe2O3 nanoparticles with 3-aminopropyltrimethoxysilane (APTMS): An attempt to investigate surface treatment on surface chemistry and mechanical properties of

polyurethane/Fe2O3 nanocomposites, Applied Surface Science, 320 60-72.https://doi.org/10.1016/j.apsusc.2014.09.026

[51] T. Kegl, I. Ban, A. Lobnik, A. Košak, (2019) Synthesis and characterization of novel γ-Fe2O3-NH4OH@SiO2(APTMS) nanoparticles for dysprosium adsorption, Journal of Hazardous Materials, 378 120764.https://doi.org/10.1016/j.jhazmat.2019.120764

[52] A. Nasiri, M. Malakootian, M.R. Heidari, S.N. Asadzadeh, (2021) CoFe2O4@Methylcelloluse as a New Magnetic Nano Biocomposite for Sonocatalytic Degradation of Reactive Blue 19, Journal of Polymers and the Environment.10.1007/s10924-021-02074-w

[53] E.M. Hussien, (2014) Development and validation of an HPLC method for tetracycline-related USP monographs, Biomed Chromatogr, 28 1278-1283.10.1002/bmc.3161

[54] X. Li, Y. Liu, C. Zhang, T. Wen, L. Zhuang, X. Wang, G. Song, D. Chen, Y. Ai, T. Hayat, X. Wang, (2018) Porous Fe2O3 microcubes derived from metal organic frameworks for efficient elimination of organic pollutants and heavy metal ions, Chemical Engineering Journal, 336 241-252.https://doi.org/10.1016/j.cej.2017.11.188

[55] N. Nasseh, B. Barikbin, L. Taghavi, M.A. Nasseri, (2019) Adsorption of metronidazole antibiotic using a new magnetic nanocomposite from simulated wastewater (isotherm, kinetic and thermodynamic studies), Composites Part B: Engineering, 159 146-156.https://doi.org/10.1016/j.compositesb.2018.09.034

[56] K.B. Babitha, V. Linsha, S. Anas, A.P. Mohamed, M. Kiran, S. Ananthakumar, (2015) Microwave assisted aqueous synthesis of organosilane treated mesoporous Si@ZnO nano architectures as dual-functional, photocatalysts, Journal of Environmental Chemical Engineering, 3 1337-1345.https://doi.org/10.1016/j.jece.2014.12.010

[57] E. Wiercigroch, E. Szafraniec, K. Czamara, M.Z. Pacia, K. Majzner, K. Kochan, A. Kaczor, M. Baranska, K. Malek, (2017) Raman and infrared spectroscopy of carbohydrates: A review, Spectrochimica Acta Part A: Molecular and Biomolecular Spectroscopy, 185 317-335.https://doi.org/10.1016/j.saa.2017.05.045

[58] G. Giani, S. Fedi, R. Barbucci, (2012) Hybrid Magnetic Hydrogel: A Potential System for Controlled Drug Delivery by Means of Alternating Magnetic Fields, Polymers (Basel), 4 1157-1169.10.3390/polym4021157

[59] N. Amirmahani, H. Mahdizadeh, M. Malakootian, A. Pardakhty, N.O. Mahmoodi, (2020) Evaluating Nanoparticles Decorated on $Fe_3O_4$@$SiO_2$-Schiff Base ($Fe_3O_4$@$SiO_2$-APTMS-HBA) in Adsorption of Ciprofloxacin from Aqueous Environments, Journal of Inorganic and Organometallic Polymers and Materials, 30 3540-3551.10.1007/s10904-020-01499-5

[60] J.A. Lopez, F. González, F.A. Bonilla, G. Zambrano, M.E. Gómez, (2010) Synthesis and characterization of $Fe_3O_4$ magnetic nanofluid, Revista Latinoamericana de Metalurgia y Materiales, 30 60-66

[61] J. Bao, Y. Zhu, S. Yuan, F. Wang, H. Tang, Z. Bao, H. Zhou, Y. Chen, (2018) Adsorption of Tetracycline with Reduced Graphene Oxide Decorated with MnFe2O4 Nanoparticles, Nanoscale Research Letters, 13 396.10.1186/s11671-018-2814-9

[62] R. Karami-Osboo, M. Maham, M. Nasrollahzadeh, (2020) Rapid and sensitive extraction of aflatoxins by Fe3O4/zeolite nanocomposite adsorbent in rice samples, Microchemical Journal, 158 105206.https://doi.org/10.1016/j.microc.2020.105206

[63] Y. Bagbi, A. Sarswat, D. Mohan, A. Pandey, P.R. Solanki, (2017) Lead and Chromium Adsorption from Water using L-Cysteine Functionalized Magnetite (Fe3O4) Nanoparticles, Scientific Reports, 7 7672.10.1038/s41598-017-03380-x

[64] J. Zhang, M.A. Khan, M. Xia, A.M. Abdo, W. Lei, C. Liao, F. Wang, (2019) Facile hydrothermal synthesis of magnetic adsorbent CoFe2O4/MMT to eliminate antibiotics in aqueous phase: tetracycline and ciprofloxacin, Environmental Science and Pollution Research, 26 215-226.10.1007/s11356-018-3452-6

[65] P. SenthilKumar, S. Ramalingam, V. Sathyaselvabala, S.D. Kirupha, S. Sivanesan, (2011) Removal of copper (II) ions from aqueous solution by adsorption using cashew nut shell, Desalination, 266 63-71

[66] A.A. Babaei, K. Ahmadi, I. Kazeminezhad, S.N. Alavi, A. Takdastan, (2016) Synthesis and Application of Magnetic Hydroxyapatite for Removal of Tetracycline from Aqueous Solutions, Journal of Mazandaran University of Medical Sciences, 26 146-159

[67] Z. Wang, X. Chen, Z. Meng, M. Zhao, H. Zhan, W. Liu, (2020) A water resistance magnetic graphene-anchored zeolitic imidazolate framework for efficient adsorption and removal of residual tetracyclines in wastewater, Water Science and Technology, 81 2322-2336.10.2166/wst.2020.283

[68] H. Yang, X. Yu, J. Liu, L. Wang, M. Guo, (2019) Preparation of Magnetic Fe3O4/Activated Carbon Fiber and a Study of the Tetracycline Adsorption in Aquaculture Wastewater, Mater. Technol, 53 505-510

[69] A. Mohammed, S. Lateef, (2019) Adsorption of tetracycline fom wastewater by using Pistachio shell coated with ZnO nanoparticles: Equilibrium, kinetic and isotherm studies, Alexandria Engineering Journal, 58.10.1016/j.aej.2019.08.006

[70] D. A.O, A. Olalekan, A. Olatunya, A.O. Dada, (2012) Langmuir, Freundlich, Temkin and Dubinin–Radushkevich Isotherms Studies of Equilibrium Sorption of Zn 2+ Unto Phosphoric Acid Modified Rice Husk, J. Appl. Chem., 3 38-45.10.9790/5736-0313845

[71] A.A. Inyinbor, F.A. Adekola, G.A. Olatunji, (2016) Kinetics, isotherms and thermodynamic modeling of liquid phase adsorption of Rhodamine B dye onto Raphia hookerie fruit epicarp, Water Resources and Industry, 15 14-27.https://doi.org/10.1016/j.wri.2016.06.001

[72] H.-T. Fan, L.-Q. Shi, H. Shen, X. Chen, K.-P. Xie, (2016) Equilibrium, isotherm, kinetic and thermodynamic studies for removal of tetracycline antibiotics by adsorption onto hazelnut shell derived activated carbons from aqueous media, RSC Advances, 6 109983-109991.10.1039/C6RA23346E

[73] J. Chang, Z. Shen, X. Hu, E. Schulman, C. Cui, Q. Guo, H. Tian, (2020) Adsorption of Tetracycline by Shrimp Shell Waste from Aqueous Solutions: Adsorption Isotherm, Kinetics Modeling, and Mechanism, ACS Omega, 5 3467-3477.10.1021/acsomega.9b03781

[74] E. Ayranci, O. Duman, (2010) Structural effects on the interactions of benzene and naphthalene sulfonates with activated carbon cloth during adsorption from aqueous solutions, Chemical Engineering Journal, 156 70-76.https://doi.org/10.1016/j.cej.2009.09.038

[75] J. Liu, B. Zhou, H. Zhang, J. Ma, B. Mu, W. Zhang, (2019) A novel Biochar modified by Chitosan-Fe/S for tetracycline adsorption and studies on site energy distribution, Bioresource Technology, 294 122152.https://doi.org/10.1016/j.biortech.2019.122152

[76] Y. Ma, M. Li, P. Li, L. Yang, L. Wu, F. Gao, X. Qi, Z. Zhang, (2021) Hydrothermal synthesis of magnetic sludge biochar for tetracycline and ciprofloxacin adsorptive removal, Bioresource Technology, 319 124199.https://doi.org/10.1016/j.biortech.2020.124199

[77] J. Miao, F. Wang, Y. Chen, Y. Zhu, Y. Zhou, S. Zhang, (2019) The adsorption performance of tetracyclines on magnetic graphene oxide: A novel antibiotics absorbent, Applied Surface Science, 475 549-558.https://doi.org/10.1016/j.apsusc.2019.01.036

[78] Y. Liu, J. Li, L. Wu, Y. Shi, Q. He, J. Chen, D. Wan, (2020) Magnetic spent bleaching earth carbon (Mag-SBE@C) for efficient adsorption of tetracycline hydrochloride: Response surface methodology for optimization and mechanism of action, Science of The Total Environment, 722 137817.https://doi.org/10.1016/j.scitotenv.2020.137817

[79] Y. Jia, J. Liu, S. Cha, S. Choi, Y.C. Park, C. Liu, (2017) Magnetically separable Au-TiO2/nanocube ZnFe2O4 composite for chlortetracycline removal in wastewater under visible light, Journal of Industrial and Engineering Chemistry, 47 303-314.https://doi.org/10.1016/j.jiec.2016.12.001

[80] Z. Lu, Z. Yu, J. Dong, M. Song, Y. Liu, X. Liu, Z. Ma, H. Su, Y. Yan, P. Huo, (2018) Facile microwave synthesis of a Z-scheme imprinted ZnFe2O4/Ag/PEDOT with the specific recognition ability towards improving photocatalytic activity and selectivity for tetracycline, Chemical Engineering Journal, 337 228-241.https://doi.org/10.1016/j.cej.2017.12.115

[81] H. Ding, G. Bian, (2015) Adsorption of metronidazole in aqueous solution by Fe-modified sepiolite, Desalination and Water Treatment, 55 1620-1628.10.1080/19443994.2014.927332

[82] M. Rathod, S. Haldar, S. Basha, (2015) Nanocrystalline cellulose for removal of tetracycline hydrochloride from water via biosorption: Equilibrium, kinetic and thermodynamic studies, Ecological Engineering, 84 240-249.https://doi.org/10.1016/j.ecoleng.2015.09.031

[83] S. Qin, L. Su, P. Wang, Y. Gao, (2015) Rapid and selective extraction of multiple sulfonamides from aqueous samples based on Fe3O4–chitosan molecularly imprinted polymers, Analytical Methods, 7 8704-8713.10.1039/C5AY01499A

[84] J. Tao, J. Yang, C. Ma, J. Li, K. Du, Z. Wei, C. Chen, Z. Wang, C. Zhao, X. Deng, (2020) Cellulose nanocrystals/graphene oxide composite for the adsorption and removal of levofloxacin hydrochloride antibiotic from aqueous solution, R Soc Open Sci, 7 200857-200857.10.1098/rsos.200857

## Figures

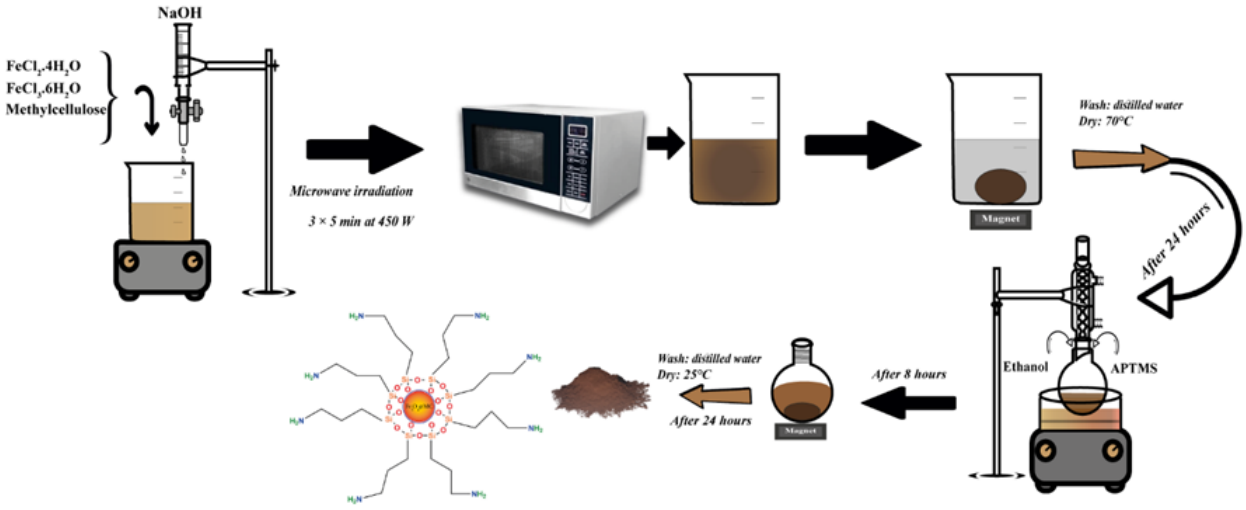


Figure 1

Schematic of preparation of Fe3O4@MC/APTMS magnetic nano-biocomposite

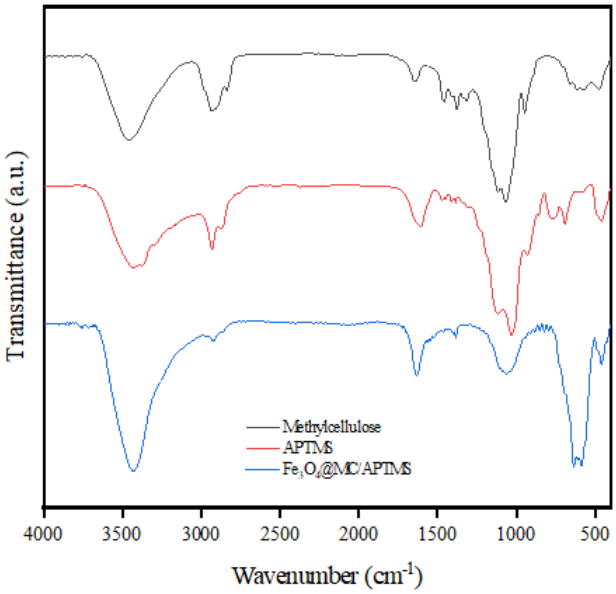


Figure 2

FTIR spectrum of Methylcellulose, APTMS and Fe3O4@MC/APTMS

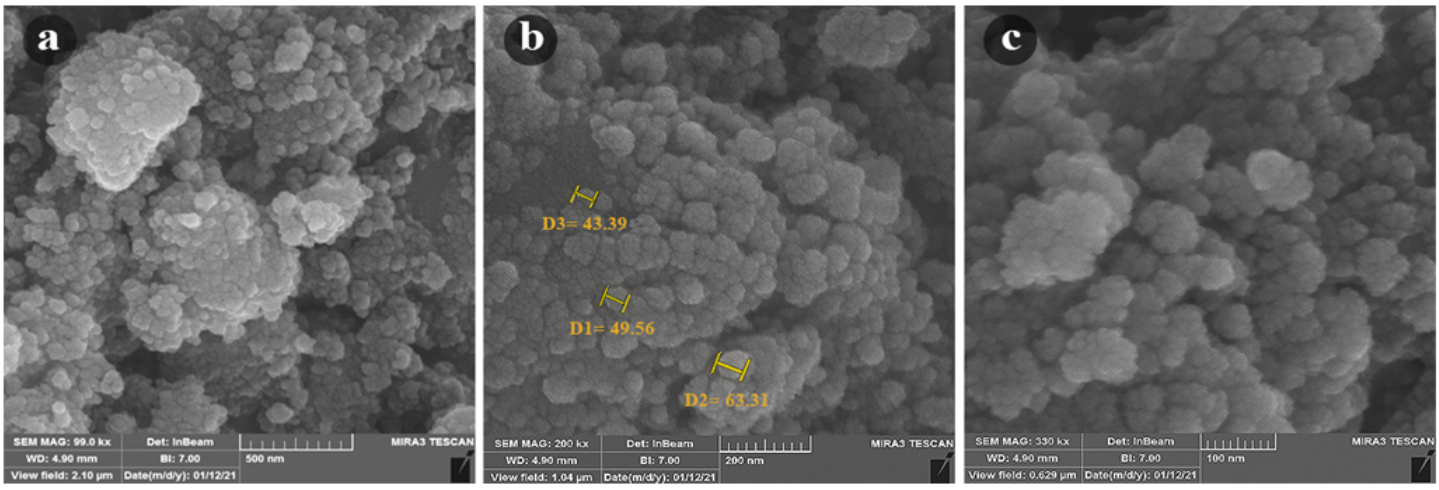


Figure 3

FESEM images of Fe3O4@MC/APTMS nano-biocomposite in 500 nm (a), 200 nm (b) and 100 nm (c) magnification

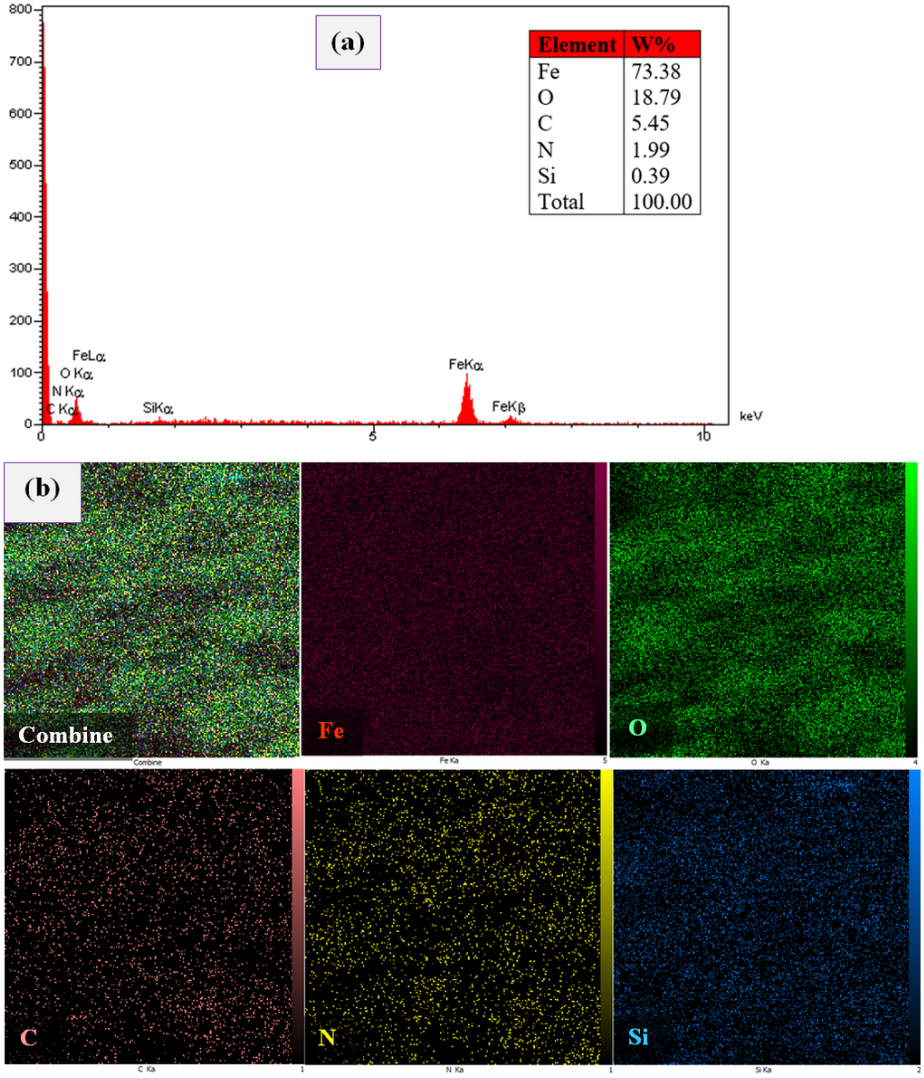


Figure 4

a) EDS patterns of the as-prepared Fe3O4@MC/APTMS nano-biocomposite b) The elemental mapping images of as-prepared Fe3O4@MC/APTMS nano-biocomposite

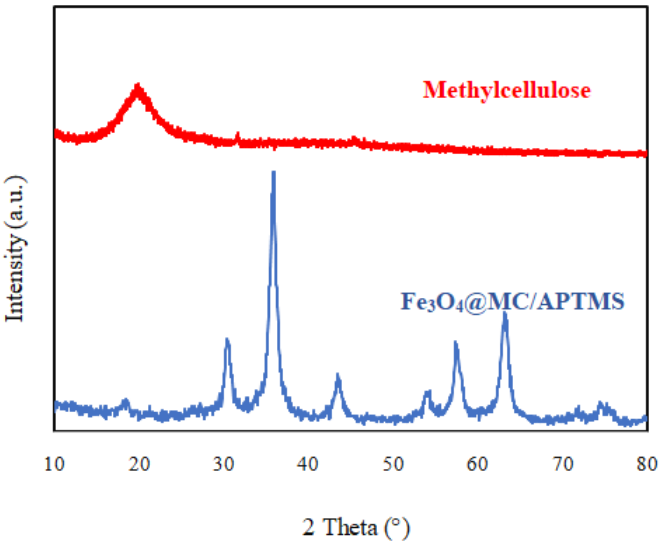


Figure 5

XRD analysis of Methylcellulose and Fe3O4@MC/APTMS magnetic nano-biocomposite

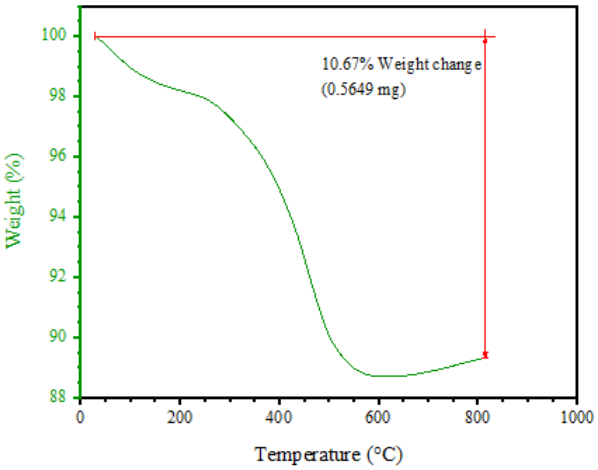


**Figure 6**

TGA analysis of Fe3O4@MC/APTMS nano-biocomposite

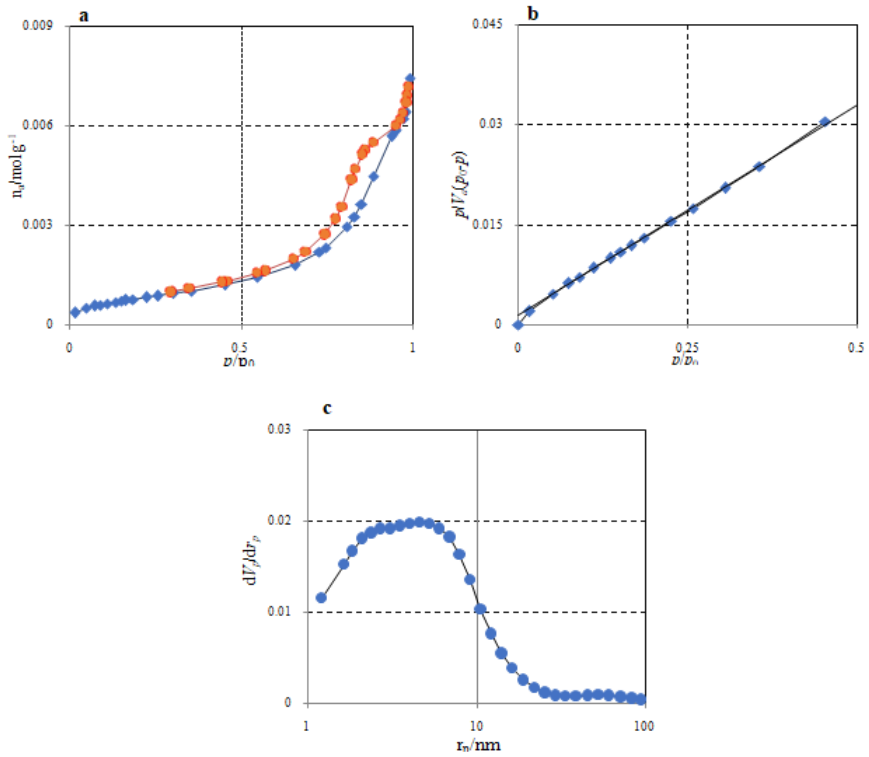


**Figure 7**

Adsorption/desorption isotherm (a), BET surface area (b), and BJH surface (c) of Fe3O4@MC/APTMS nano-biocomposite

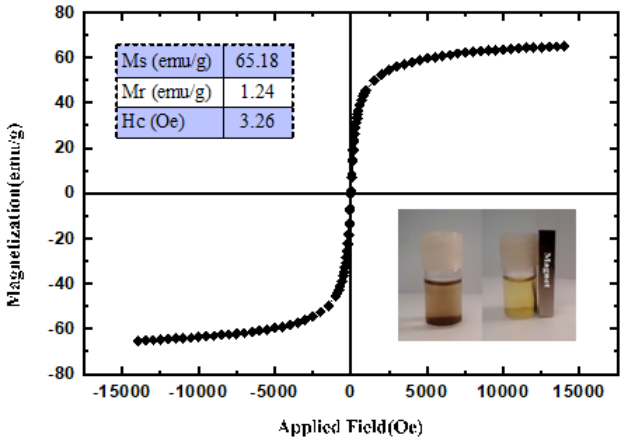


Figure 8

VSM magnetization curve of Fe3O4@MC/APTMS nano-biocomposite

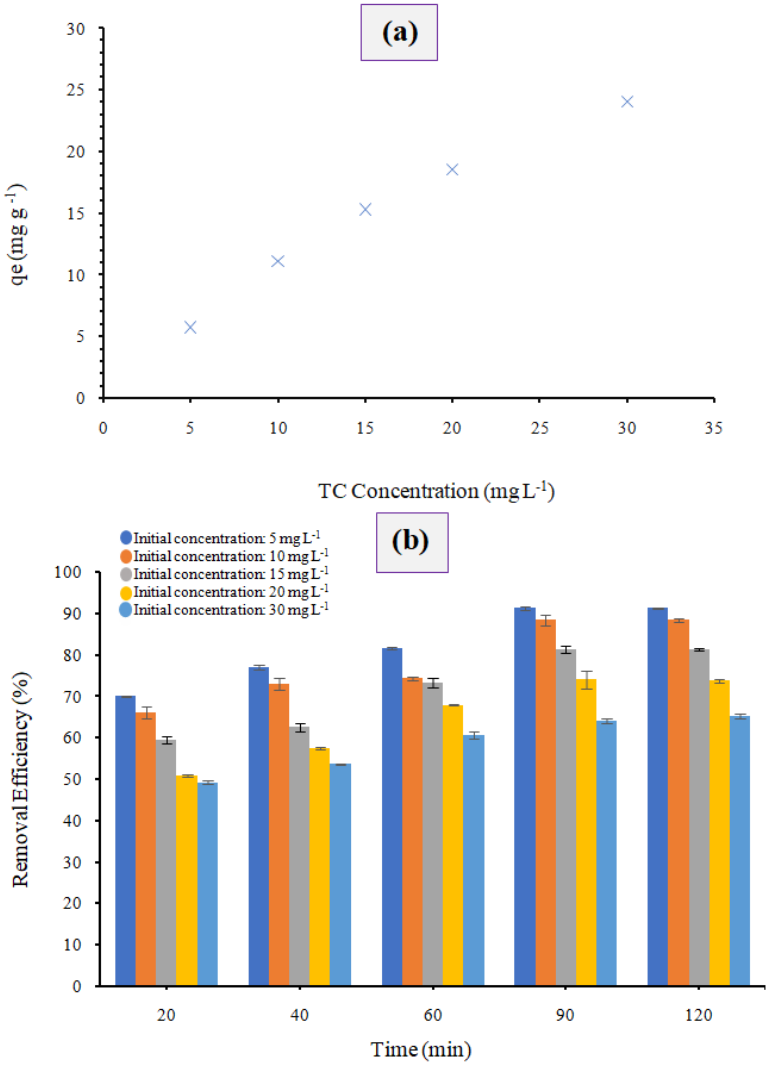


Figure 9

a) Changes in the adsorption capacity at different TC concentrations b) Effect of TC initial concentration on removal efficiency (Adsorbent dose: 80 mg L-1, and pH: 6)

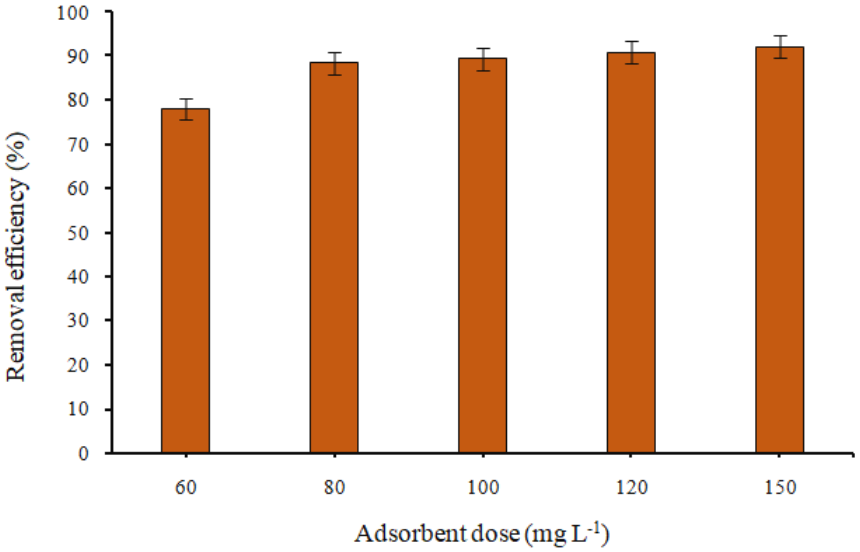


Figure 10

Effect of magnetic nano-biocomposite dosage on TC removal efficiency (initial TC concentration)

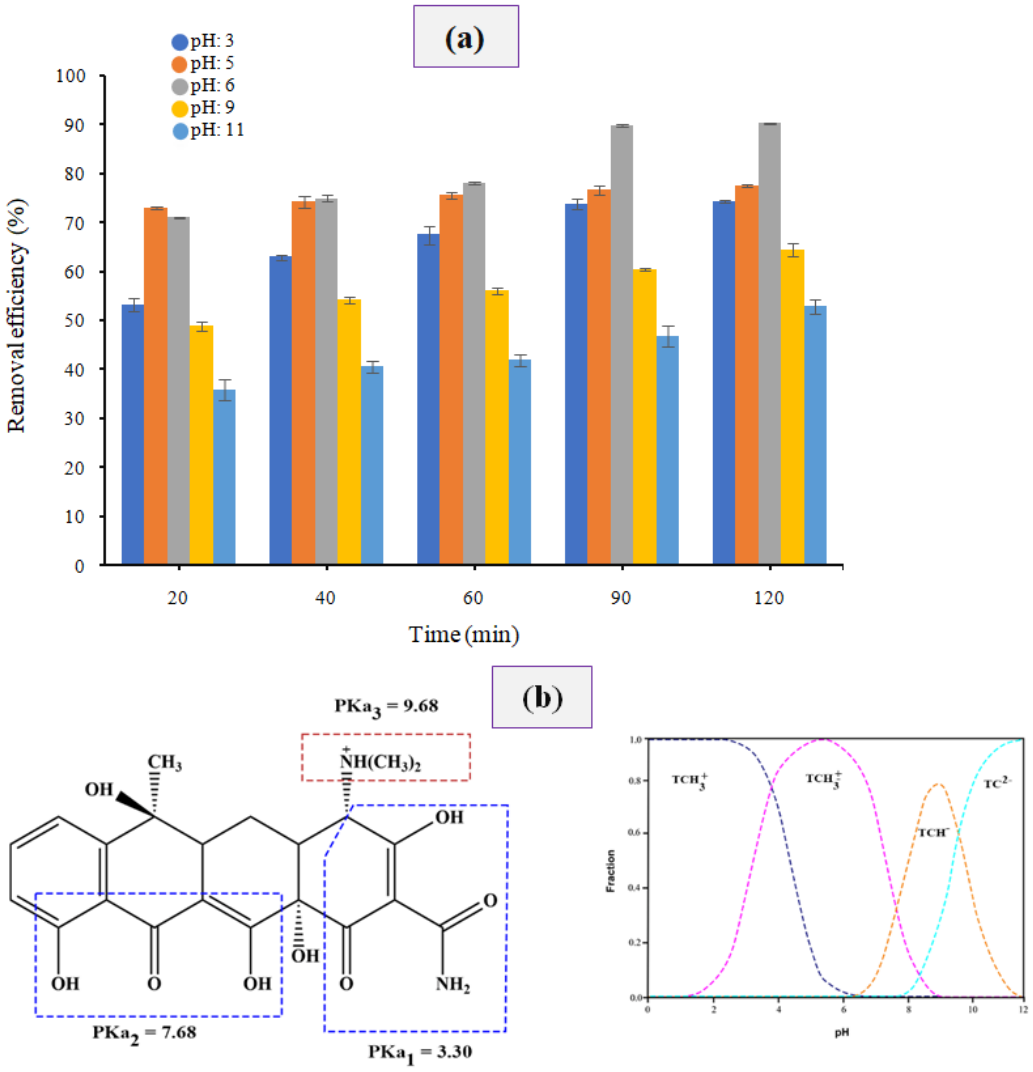


Figure 11

a) Effect of pH on TC removal efficiency in different times (Initial TC concentration:10 mg L-1 and Adsorbent dose: 80 mg L-1) b) Tetracycline ionization at different pHs

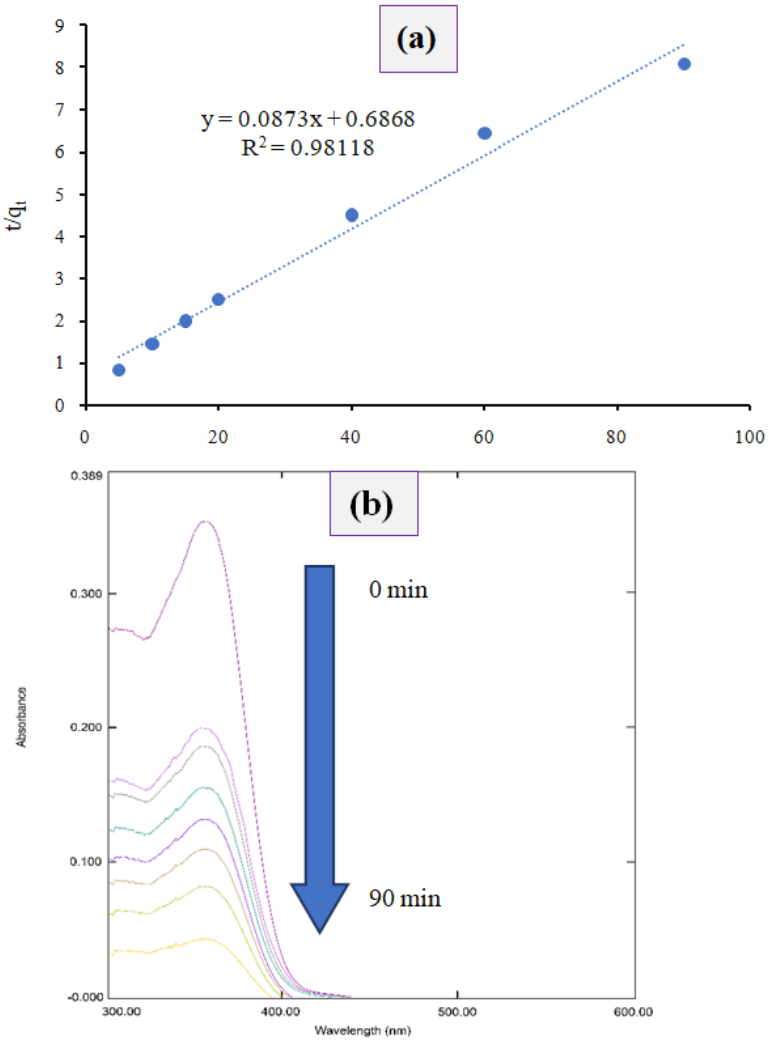


Figure 12

a) Pseudo-second order kinetic model diagram b) Changes in the adsorption spectra of TC for 90 min (Initial TC concentration: 10 mg L-1, Adosrbent dose: 80 mg L-1, pH= 6)

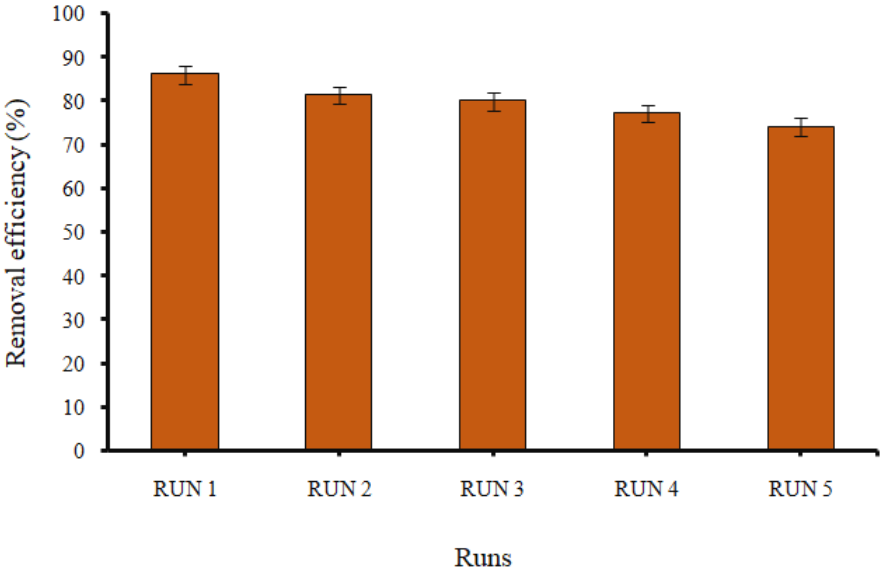

Figure 13

Recycling and reuse of the Fe3O4@MC/APTMS for TC adsorption (initial TC concentration)

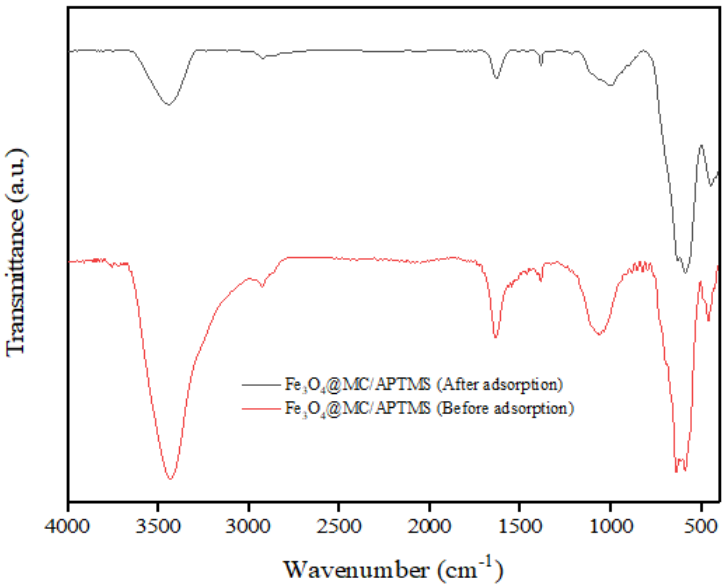


Figure 14

FTIR of Fe3O4@MC/APTMS before and after TC adsorption